Complex analysis of laser induced contamination in high reflectivity mirrors

Tomas Tolenis[1,*], Saul Vazquez[1], Lukas Ramalis[2], Mojmír Havlík[1], Adrien Chauvin[1], Anna Těreščenko[1], Shirly Espinoza[1], Anna Fučíkova[3], Jakob Andreasson[1], Irena Havlickova[1], Jan Hřebíček[1], Bedrich Rus[1] and Daniel Kramer[1]

[1]ELI Beamlines-ERIC, Za Radnicí 835, Dolní Břežany, Czech Republic

[2]Center for Physical Sciences and Technology, Savanorių ave. 231, LT-02300, Vilnius, Lithuania

[3]Faculty of Mathematics and Physics, Charles University, Ke Karlovu 3, 121 16, Prague 2, Czech Republic

*Corresponding author: tomas.tolenis@eli-beams.eu

Abstract

Operation of high power and high repetition rate laser systems are commonly disrupted by the failure of optical components. Optical coatings in vacuum systems accumulate laser induced contamination (LIC) and are damaged afterward. Currently, only active LIC mitigation methods involving plasma cleaning or oxygen injection in the system are used, which require additional interventions and can disrupt the regular operation. The presented investigation aims to study the multilayer coating design influence on the formation of laser induced contamination for dielectric high reflectivity Bragg mirrors. The manipulation of electric field enhancement on the surface and the material of the last layer revealed that silica tends to accumulate more surface contamination than hafnia materials. Also, the size of the affected area linearly depends on the strength of the E-field at the coating surface. These findings suggest that optimizing coating design—specifically by controlling the E-field distribution and top-layer material—can minimize LIC growth, potentially extending the lifespan of optical components in high-power laser applications, including space and industrial systems.

Keywords: Optical coatings, Laser induced contamination, High power lasers

This peer-reviewed article has been accepted for publication but not yet copyedited or typeset, and so may be subject to change during the production process. The article is considered published and may be cited using its DOI.

10.1017/hpl.2025.10069

1. Introduction

High power laser systems are often used in a vacuum environment to avoid non-linear phenomena [1] or when applications are in space [2]. Despite the sub-threshold (for one pulse) irradiation level, the performance of optical components is still degrading after the long exposure. Such laser induced behavior is especially common and becomes an increasing problem at MHz or higher frequency, where cumulative laser-induced effects lead to a progressive decline in optical performance. Irradiation by ultrashort pulses can generate self-trapped excitons, which may form color centers in transparent dielectrics [3]. Following pulses only enhance such behavior and the laser-induced damage (LID) occurs (see Fig 1. a)). The fatigue effect in optical coatings is drastically reducing their lifetime. It mainly depends on materials band gap and defect density, which can be partly controlled by changing the coating design and by mitigating defect sources [4]. Unfortunately, despite the minimized fatigue effect influence, surfaces are still being damaged due to laser induced contamination (LIC) (see Fig. 1 c)). Organic contamination within the vacuum chambers can originate from the outgassing of optomechanical parts in laser systems. Such molecules can be adsorbed (or even absorbed) directly on the optical surfaces or can be dragged by the intense light pulses and deposited on the irradiated surfaces. Nucleation of hydrocarbon molecules induces light losses in transmittance and reflectance. When the absorption reaches a certain level, catastrophic damage is initiated. LIC is common in most of the high power laser systems which work under vacuum conditions or in space. It can cause a loss in the output power and induce laser beam quality issues. Laser pulses with high photon energies or with ultrafast pulses enabling multiphoton absorption can deplete the deposited molecules of hydrogen and thus form carbonized [5].

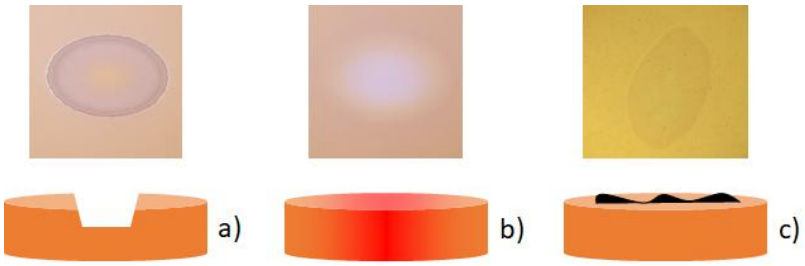

Fig. 1. The schematics of laser-induced a) damage, b) discoloration and c) contamination. The figures at the top show Nomarski optical microscopy images of the corresponding laser induced modes in multilayer dielectric mirrors. Figures at the bottom represent the principal change in coatings structure.

Initiated LIC is one of the major limiting factors in high intensity ultrafast laser systems. Therefore, mitigation procedures are crucial for successful operation. Currently, there are two main strategies for cleaning or avoiding laser induced contamination and both of them use oxygen ions. The first one uses Radio Frequency (RF) plasma and the second one uses UV light or ultrafast pulses. Bombardment of contaminated optics surfaces by energetic particles using plasma is currently a standard practice in facilities like ELI ERIC [6]. The energy of plasma particles must be sufficient for the removal of the carbonous layer, but should not exceed the bonding energy of the coatings surface. Such a procedure can take up to more than ten hours and interrupts daily

https://doi.org/10.1017/hpl.2025.10069 Published online by Cambridge University Press

procedures. Injection of oxygen in a vacuum chamber and ionizing it by UV light or laser beam itself creates radicals, which react with the contamination layer. Previous investigations indicate [7] a threshold behavior, where sufficient amount of oxygen starts cleaning or prevents the contamination. Such an approach is used for laser systems in space applications. Both solutions allow to minimize the contamination influence, but require additional active intervention in the setup.

It was shown in recent papers that LIC behavior, namely the growth rate, differs in separate materials [8, 9]. Experimental results indicate that silica material has the highest contamination growth rate compared to materials such as hafnia or niobia. Unfortunately, to the author's knowledge, only comparisons between single layers have been demonstrated. During the investigation of multilayers the electric field (E-field) distribution was found to play an important role [10, 11] for LID. Depending on the strength of E-field within the layers of different materials the laser induced damage or color changes were detected at different fluences. Therefore, it is crucial to investigate the influence of E-field distribution on the LIC as well.

In the current paper, we aim to explore the mitigation of the LIC effect by changing the coating design of high reflectivity mirrors. Coatings with different materials for the top layer and different E-field distributions at the surface to vacuum interface were investigated by optical microscopy for visual comparison and by imaging ellipsometry for quantitative insights into the optical property changes.

2. Methods

For the investigation of how the top layer material and the E-field distribution within the multilayer dielectric mirrors influence the formation of LIC, four designs were devised. The base structure of all samples consisted of quarter-wavelength-optical-thickness (QWOT) layers. A total of 31 layers of hafnia and silica were kept at the same optical thickness and only the last, namely 32^{nd}, layer was different in each design. First 31 layers were all equal to one QWOT at the wavelength of 810 nm for the 45 deg angle of incidence. Therefore, the physical thickness of hafnia was modeled to be 121 nm, and for silica 170.6 nm. For the first sample, only 31 layers were deposited, keeping the last layer of the design as hafnia. For the other three designs, the last layer was silica, but with the different optical thicknesses: 1 QWOT, 1.5 QWOT and 2 QWOTs. Therefore, all four samples were named as “0L”, “1L”, “1.5L” and “2L”. The E-field distributions of all designs are presented in Fig. 2.

https://doi.org/10.1017/hpl.2025.10069 Published online by Cambridge University Press

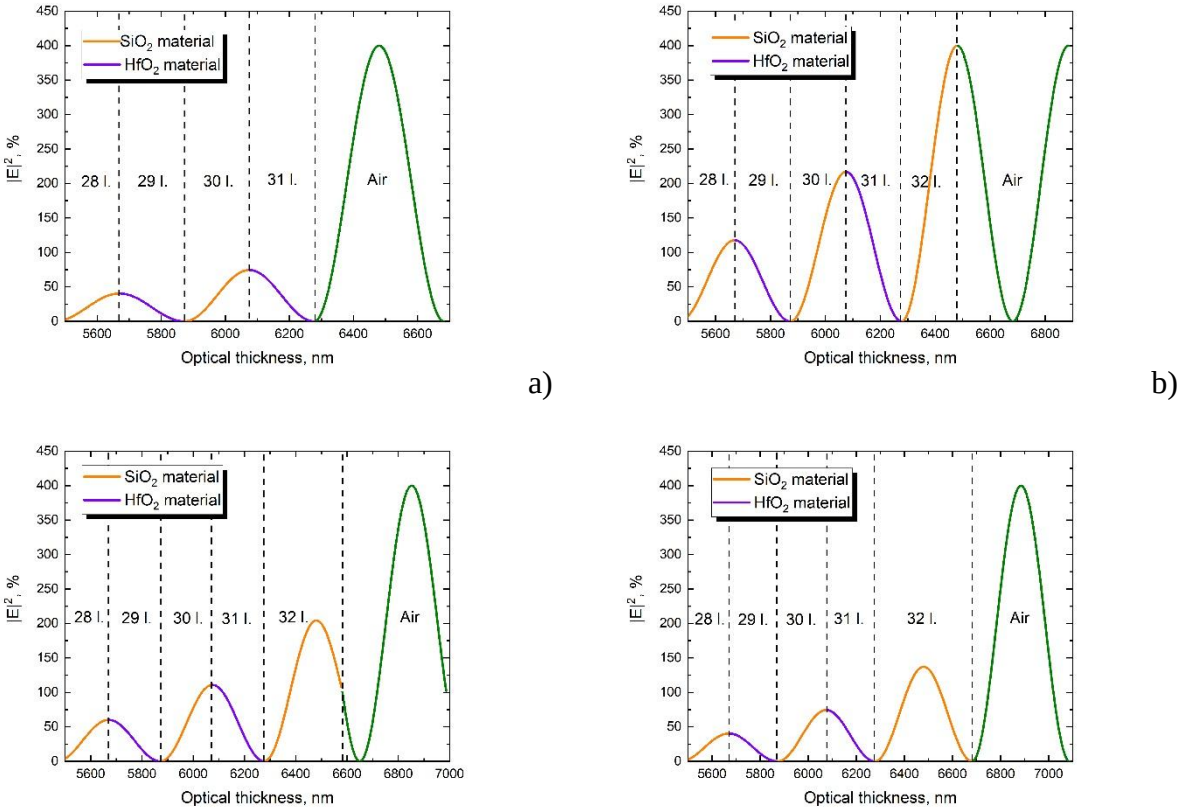

Fig. 2. E-field distributions within the last four or five layers of a) “0L”, b) “1L”, c) “1.5L” and d) “2L” designs.

All experimental samples have been deposited using electron beam evaporation technology. VERA 1100 (VTD, Germany) deposition plant has been used for all processes. Hafnia and silica layers have been coated by evaporating silica granules (1.5 – 3.5 mm, Umicore) and (1 – 4 mm, Umicore) materials from copper crucibles. Depositions have been performed under the vacuum conditions of (1.4×10^{-5} Pa) and by injecting oxygen of 100 sccm for oxidation. Evaporation speed and thickness of each layer have been controlled by quartz crystal monitoring. Deposition rates were maintained at 3 Å/s and 3 Å/s for silica and hafnia, respectively. Plasma source IS300 (CCR Technology GmbH) was used during the deposition process with the power of 2500W.

For the laser-induced contamination, all experimental samples have been tested using femtosecond pulsed laser (τ =46 fs, $\lambda = 810$ nm, $f = 1$ kHz) Astrella (COHERENT). Each sample was irradiated at one site with a fixed fluence of 350 mJ/cm^2, which was attenuated by a half-waveplate and polarizer combination. Samples were also tested at 150 mJ/cm^2 fluence and no LIC was detected. From our previous measurements of similar coatings we know that the threshold of laser induced damage can be somewhere between 500 mJ/cm^2 and 1 J/cm^2 depending on E-field distribution. This value may be reduced using several million pulses. Therefore, the irradiation at lower values, namely 350 mJ/cm^2, was considered as safe value for investigation. The laser beam

https://doi.org/10.1017/hpl.2025.10069 Published online by Cambridge University Press

was directed to the vacuum chamber, which was pumped to the level of 10^{-6} mbar using mechanical and turbomolecular pumps. The beam size was set by an f = 800 mm concave mirror and fixed at 360 µm in diameter. The direct beam profile was recorded before and after the experiments with a CCD camera by tilting the sample 90 degrees with respect to the analysis position (shown in Fig.3) and during the tests with a leak camera. Samples were irradiated at 45 deg angle of incidence. Each site was irradiated at 1 kHz for three hours with a total of 10.8 million pulses. Prior to the measurements, residual gas analysis (RGA) was recorded to follow the vacuum quality by a quadrupole mass spectrometer (Extorr). The setup of LIC system is presented in Fig. 3.

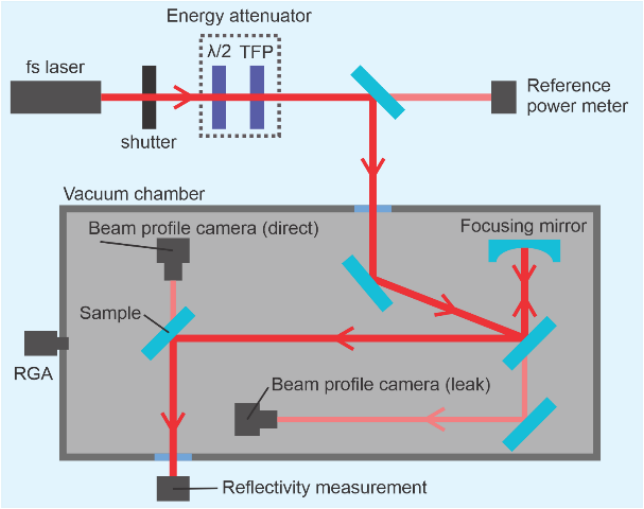

Fig.3. Schematic of the experimental setup used for the LIC test.

Qualitative analysis of LIC has been performed by optical microscope LEXT OLS5100SAF (OLYMPUS). Different magnifications have been used for general overview of irradiated sites and characteristic features. All images have been obtained in reflection mode and using Differential Interference Contrast (DIC) microscopy.

Surface of "1L" experimental sample was also analysed using atomic force microscope (AFM). For measuring the sample we used AFM Nanowizard 3 from JPK Instruments, Germany (now Bruker, USA), operated via control station VortisTM and Advanced SPMControl and controlled via JPK SPM Desktop software, which is placed on top of inverted microscope Olympus IX73. Data were processed with JPK Data processing software. The sample has been measured in AC mode with the use of Acta cantilever from AppNano.

Reflectance of all experimental samples were measured by Photon RT spectrophotometer (EssentOptics). Measurements have been performed in clean-room environment, at room temperature. Reflectances at 45 deg angle of incidence were measured for S and P polarizations using linearly polarized light.

Spectroscopic Imaging Ellipsometry (SIE) measurement of the ellipsometric angles Ψ and Δ were performed on the multilayer dielectric mirrors with an imaging ellipsometry spectrometer

https://doi.org/10.1017/hpl.2025.10069 Published online by Cambridge University Press

EP4 (Accurion) in nulling mode. The objective of the EP4 was a Nikon CF Plan SLWD 10X (NA = 0.21). All the experiments were performed in ambient conditions at room temperature, across 450-1000 nm wavelength range. The monochromatic light was provided by a laser-driven Xenon lamp and a monochromator. Measurements were performed with equally spaced steps of 5 nm at an angle of incidence (AOI) of 50°. The principal schematics and main components of the imaging ellipsometry setup are shown in Fig. 4.

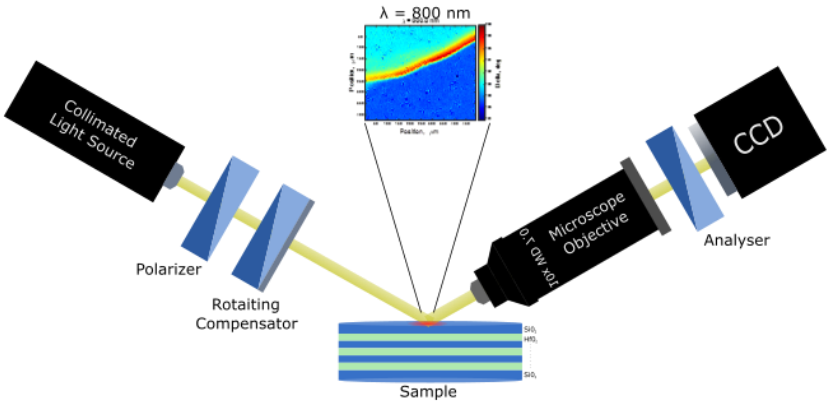

Fig. 4. Principal schematics of scanning imaging ellipsometry used for detecting LIC sites on experimental samples.

For SIE, the light passes through a polarizer for linear polarization and then through a compensator to produce elliptically polarized collimated light such that the light reflected from the sample is again linearly polarized. The reflected light passes through a 10x objective and an analyzer to a CCD camera enabling a lateral resolution of approx. ≈ 1 μm. In an appropriate coordinate system, the complex reflectance matrix is described by $\rho = r_p/r_s = \tan\Psi \cdot e^{i\Delta}$, with r_p or r_s the amplitudes of the parallel (p) and orthogonal (s) components of the reflected light normalized to their initial amplitudes (amplitude of incoming light) and the ellipsometric angles Ψ and Δ, respectively [12].

In the SIE mode, the intensity of the reflected light is minimized by a 90° alignment of the analyzer with respect to the reflected light fulfilling the nulling condition [13, 14] for the selected region of interest (ROI). The ROI is a certain area on the sample under investigation and therefore, just a reduced number of pixels on the CCD camera will be used to adjust for the nulling conditions. The ROI can be as small as the area of an individual pixel on the CCD. Here, a ROI is defined such that selected pixels are accumulated to achieve a sufficient signal to noise ratio. The area of the sample has been divided into the 2 equally sized ROIs with a lateral size of about 100 μm × 50 μm. In this way, the Ψ- and Δ- values, representing amplitude and phase difference between the respective polarization components, are taken individually for different ROIs on the sample with a high lateral resolution given by the overall resolution of the optics in the reflected light beam. For SIE maps, the polarizer and analyzer-angles are determined by fulfilling the nulling condition for each ROI.

https://doi.org/10.1017/hpl.2025.10069 Published online by Cambridge University Press

3. Results and discussion

Each of the experimental samples is a Bragg mirror at 810 nm wavelength. Therefore, the spectral properties near the Bragg region should be similar. Reflectance measurements of experimental samples are presented in Fig. 5. The reflectance at the wavelength of 810 nm exceeds 99.5 % for S polarization for all the samples at the angle of 45 deg. The characteristics of the spectra within the Bragg zone is typical for QWOT-based dielectric mirrors. Further from the reflectance zones, the reflectance curves differ due to individual thicknesses of the last layer in each of the samples.

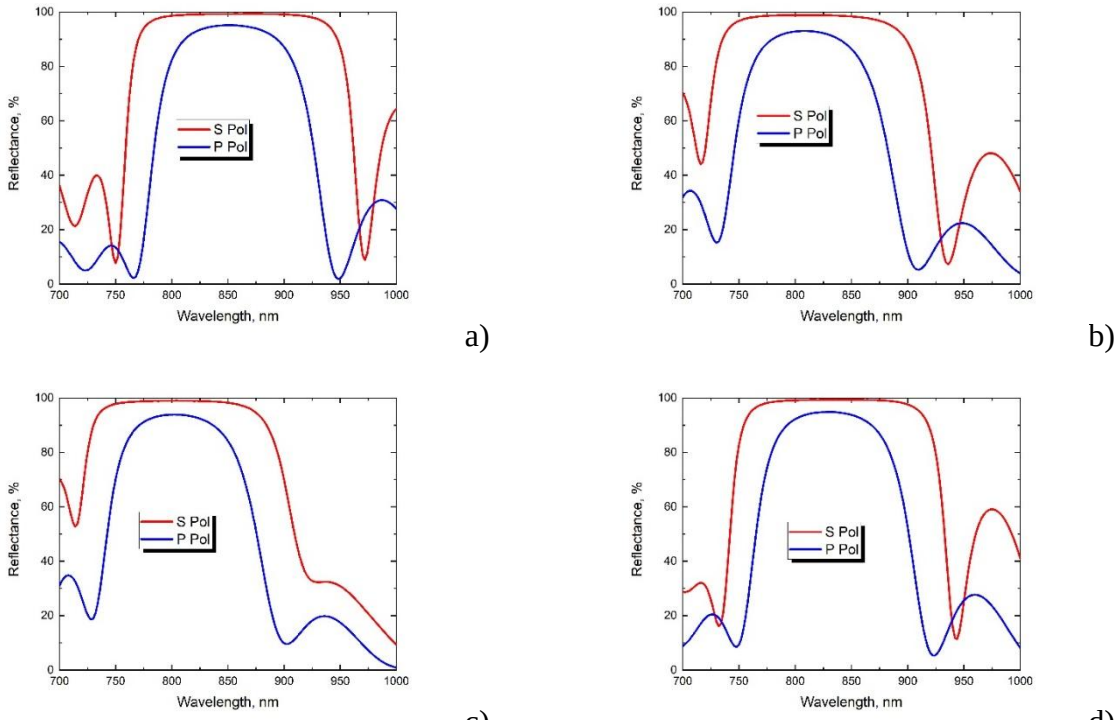

Fig. 5. Spectrophotometric measurements for S and P polarized light reflectance of a) “0L”, b) “1L”, c) “1.5L” and d) “2L” experimental samples before the laser irradiation.

Laser-induced-contamination areas are presented in Fig. 6. Each irradiated spot is plotted with corresponding beam profile measurements and zoomed on the edge of the image for better observation. Irradiation of the sample with hafnia layer on top (“0L”, Fig. 6a) resulted in a barely visible contamination spot. Sharper discoloration is seen at the edges, but zooming by 100 magnification long focal lens system showed no distinctive difference between the two areas. The size of the contaminated area was determined by fitting the elliptical shape, which had 493 μm and 821 μm minor and major axes, respectively, in this case. A more distinctive irradiation imprint can be seen for the “1L” sample (Fig. 6b). The discoloration of induced contamination is gradually changing going from the center to the edge. The size of the observed contamination was 734 μm and 1223 μm for minor and major axes, respectively. For the experimental sample “1.5L” (Fig. 6c), the irradiation imprint is also distinctive and clear edges are observed. The induced

https://doi.org/10.1017/hpl.2025.10069 Published online by Cambridge University Press

contamination is seen as discoloration of the area with the size of 576 μm and 960 μm for minor and major axes, respectively. The last sample, namely "2L" (Fig. 6d), contained a darkened irradiation imprint with a similar size to the "0L" sample case. The zoomed image indicates the rough structure of the contamination.

According to the beam profile measurements, the peak intensity was at the center of the spot following a Gaussian profile. Such a profile was not embedded in any of the experimentally observed features during the irradiation for three hours. On the contrary, the edges of irradiated spots were affected the most.

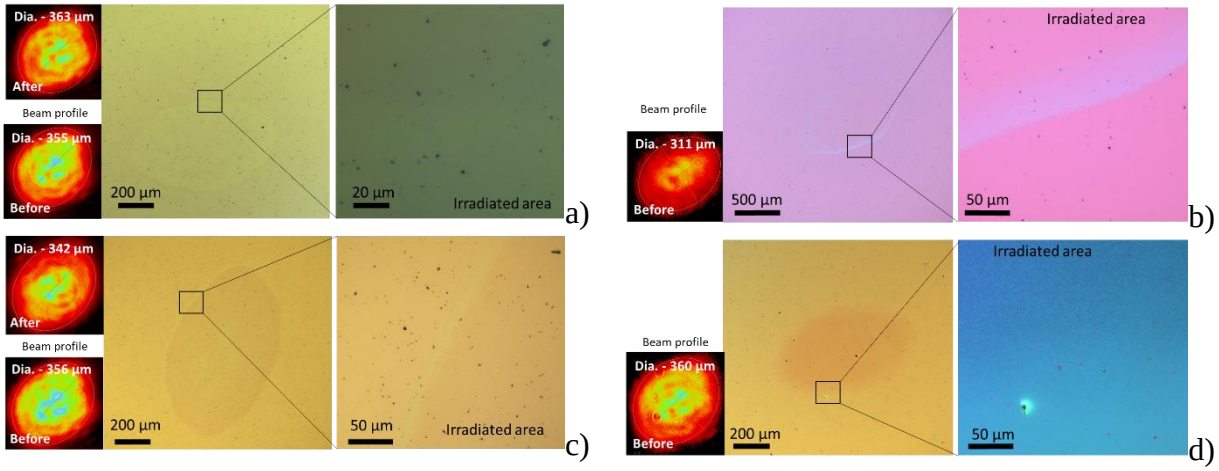

Fig. 6. Images of LIC of a) "0L", b) "1L", c) "1.5L" and d) "2L" experimental samples obtained by DIC microscopy. For the observation of the full irradiated spot, magnifications of 5x or 10x were used by standard lens systems. In case of the zoomed areas, long focus lenses of 50x or 100x were used. Small images on the left are beam profile measurements by CCD camera in each case before or after the irradiation (normal to beam propagation).

Imaging ellipsometry measurements of the area containing clear and irradiated surfaces are presented in Fig. 7. Results are presented only at 800 nm wavelength, which is within the Bragg zone for all the samples. The data at other wavelengths, which are close to the reflection zone, are similar. Absolute value of Delta (Δ) parameter is different for each of the samples, but the differences of *max* and *min* in graph colorbars (range of 16 degrees) were kept the same for all the samples for better comparison. Differences of irradiated areas are visible in all cases. The largest difference was detected for the sample "1L" (Fig. 7b). A gradual increase of the delta parameter was mostly observed at the edge of the contaminated area (Fig. 7a-d).

https://doi.org/10.1017/hpl.2025.10069 Published online by Cambridge University Press

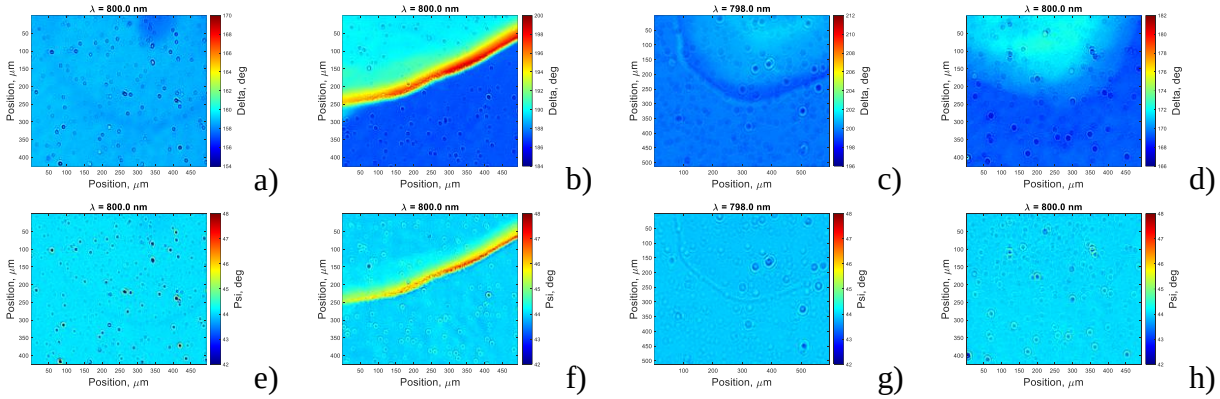

Fig. 7. Imaging ellipsometry measurement maps at 800 nm wavelength of Delta parameter for a) "0L", b) "1L", c) "1.5L" and d) "2L" experimental samples and of Psi parameter for e) "0L", f) "1L", g) "1.5L" and h) "2L" experimental samples.

Δ (Delta parameter): represents the phase difference between the reflected p- (parallel) and s- (perpendicular) polarized components of light after the reflection. An increase or decrease of Δ indicates a modification in the optical structure of the material. LIC modifies the surface dielectric properties, leading to a shift in Δ. For quantitative comparison, cross-sections of Delta parameter surface maps were plotted (see Figure 8). The values were collected by taking averaged data from 30 μm width area (in the horizontal direction) and plotting them at each vertical coordinate. The changes of the Delta parameter are minimal for "0L" sample and fluctuate within <1 deg throughout the scan length (Fig. 8a). Delta for "1L" sample (Fig. 8b), on the other hand, has largest variation between affected areas and clean surface (~10 degrees at the edge of the irradiated area and ~2.5 degrees for the central part of the contaminated spot). Variation of Delta for "1.5L" sample (Fig. 8c) is ~1 degree and for "2L" (Fig. 8d) is - ~3 degrees.

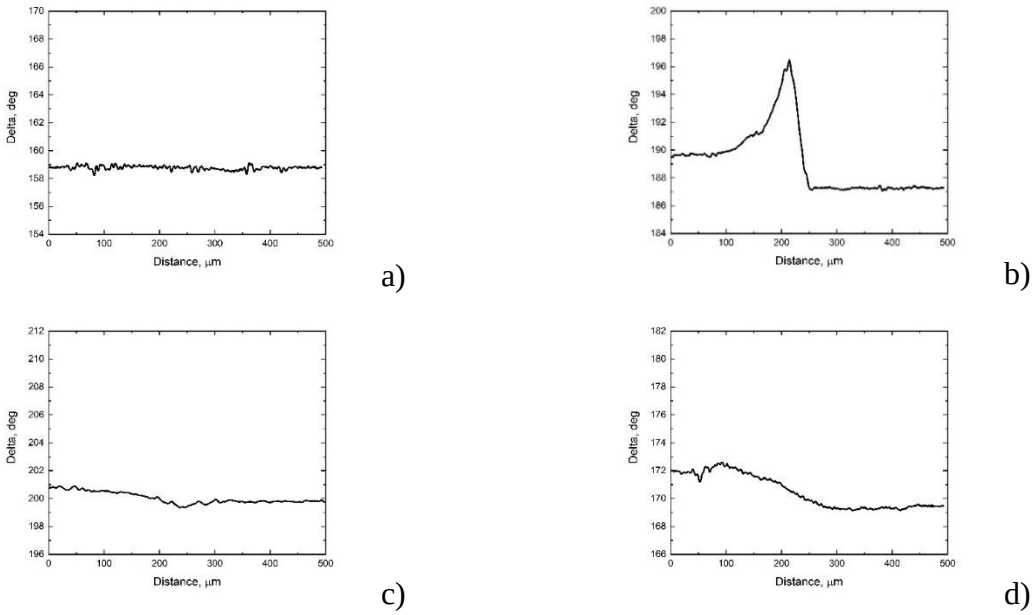

https://doi.org/10.1017/hpl.2025.10069 Published online by Cambridge University Press

Fig. 8. Cross-section of Delta parameter for a) “0L”, b) “1L”, c) “1.5L” and d) “2L” experimental samples.

Ψ (Psi parameter): Represents the ration of amplitude between the p- and s- light components after reflection. A decrease in Ψ indicates an increase in absorption or scattering due to surface contamination. Psi value for all the samples remains close to 45 degrees and varies only within +/- 5 degrees (Fig. 7e-h). Largest fluctuation is visible for the “1L” sample (Fig. 7 f), consistent with the strongest LIC effect. The increase in Psi parameter to the level of ~48 degrees is located only at the edge of the irradiated area. Minimal Ψ variation (<1°) is observed in “0L” and “1.5L”, confirming reduced contamination.

Ellipsometric measurements were taken beyond the Bragg region, for a broad spectral range – from 450 nm to 1000 nm. The spectra close to the Bragg zone of the unaffected and irradiated sample areas are shown in Fig. 9. The data were collected by averaging 30 μm × 30 μm spots of the maps (whole maps shown in Fig. 7) for both cases (see Fig. S1 in supplementary file). Differences between the Delta spectra are minimal for “0L” sample (Fig. 9a) and “1.5L” (Fig. 9c) within the Bragg spectral zone. In case of “1L” (Fig. 9b) and “2L” (Fig. 9d), the differences reach four and three degrees, respectively. Differences between irradiated and unirradiated surface areas are presented as insets of the respective graphs in Fig. 9. The Psi parameter remained similar (Fig. S2 in supplementary file) within the Bragg spectral zone for all the experimental samples. This suggests that LIC introduces spectral dispersion, altering the surface optical properties beyond the primary reflection band.

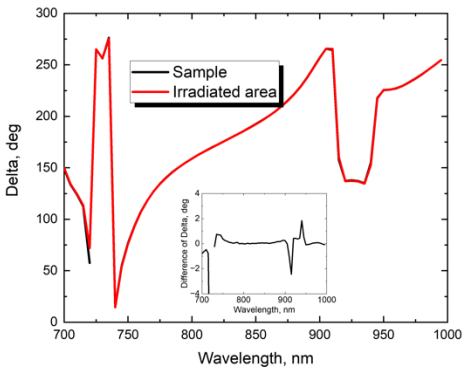

a)

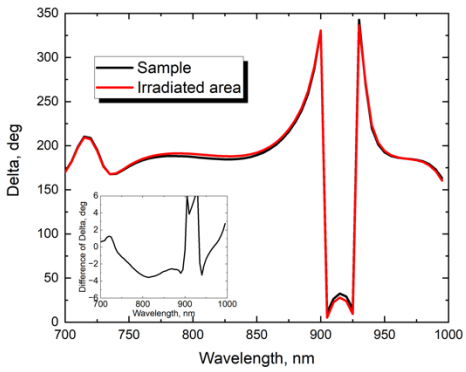

b)

https://doi.org/10.1017/hpl.2025.10069 Published online by Cambridge University Press

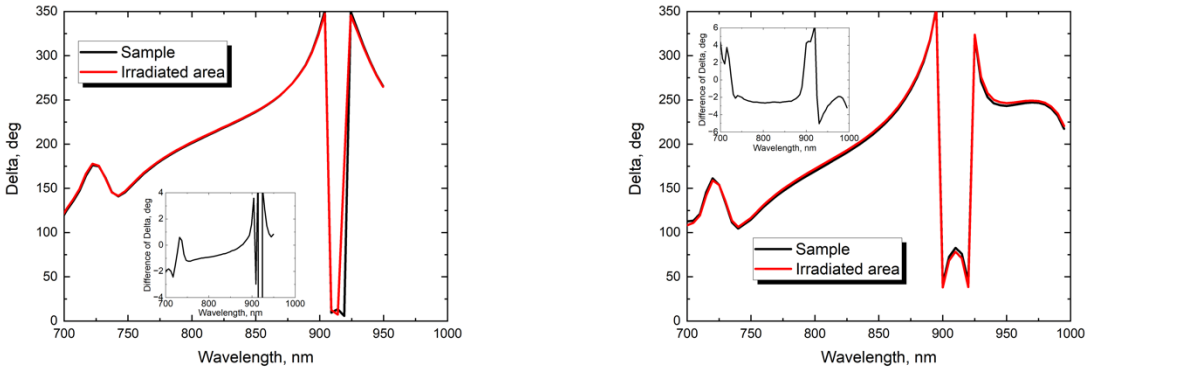

Fig. 9. Averaged spectroscopic ellipsometry Delta parameter for irradiated and unirradiated zones of a) "0L", b) "1L", c) "1.5L" and d) "2L" samples. Insets in each figure indicate the difference between the two respective datasets.

The thickness distribution of LIC for the "1L" experimental sample was analyzed using AFM. The surface map for the area at the edge of the irradiated site is presented in Fig. 10. Two height line scans were analyzed for comparison of height differences between the middle of the irradiated area (R1), edge (R2 and R3) and the sample outside the LIC site (R4). The average values of height distribution for R1 and R2 ranges are 1.5 nm and 3.8 nm, respectively. In the second line scan, the average values of height distribution for R3 and R4 ranges are 5.4 nm and 1.8 nm respectively. Therefore, the difference in surface heights between the center and edge of the LIC site is 2.3 nm. At the same time, the difference between the edge of the LIC site and the clear area is 3.6 nm. A 3D plot is presented in Fig. S3 of the supplementary file.

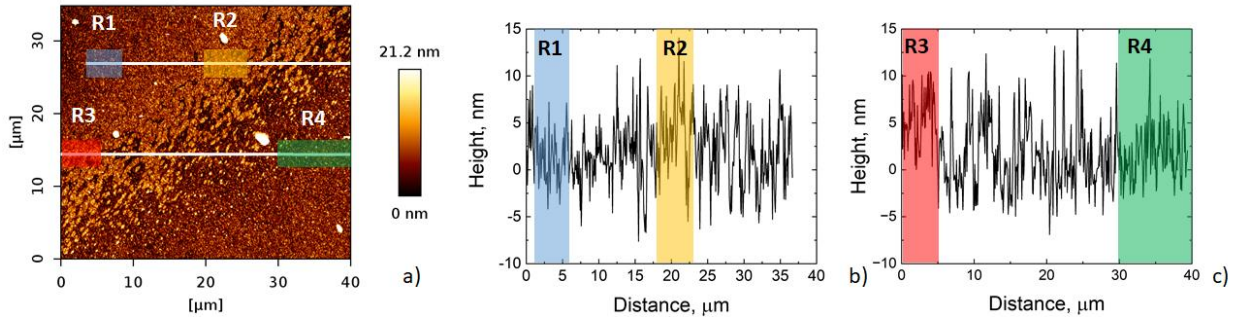

Fig. 10. AFM analysis of "1L" experimental sample shown as a) image of surface topography with indicated ranges in two line scans: R1, R2, R3 and R4. Cross-sections with height distributions are shown in b) and c).

4. Discussion

The pumping process took about 1h to reach a pressure of 10^{-6} mbar. The chamber was previously vented through the primary scroll pump to obtain contamination levels common to many labs. No further cleaning after the pumping has been carried out. To get insight into the contamination, residual gas analysis (RGA) was sampled when the working pressure was reached

https://doi.org/10.1017/hpl.2025.10069 Published online by Cambridge University Press

prior to each LIC experimental run. The typical RGA spectrum is displayed in Fig. 11. The series of all RGA measurements during the experiments are presented in supplementary material (Fig. S6) to show that contamination conditions during the experiments were similar.

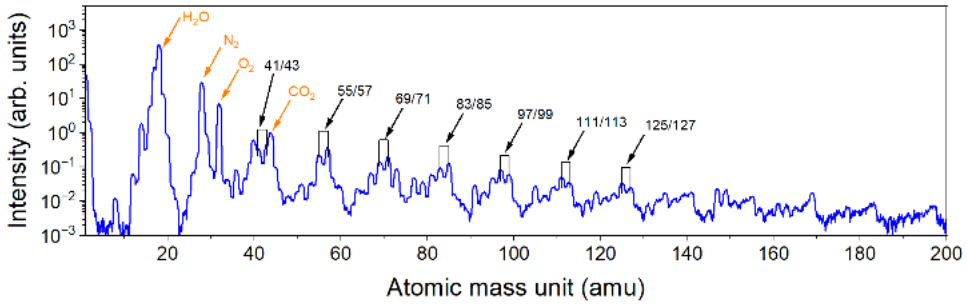

Fig. 11. RGA spectrum of the LIC chamber measured at 10^{-6} mbar prior to the experiments. Spectrum is normalized to the CO_2 peak at 44 amu.

The RGA spectrum shows a presence of H_2O, N_2, O_2, and CO_2, which is expected during the pumping of a chamber from ambient air. Moreover, we can notice contamination by hydrocarbons. These hydrocarbons give fragments of C_3H_5 and C_3H_7 at 41 and 43 amu, respectively. The peaks are separated by 14 amu when going to higher atomic mass, corresponding to the mass increase of CH_2. The doublet can be clearly seen up to 125/127 amu indicating the presence of long molecular chains and elevated amount of hydrocarbon contamination in general. Moreover, the ratio between the CO_2 and hydrocarbon (C_3H_7) peaks, located at 44 and 43 amu respectively, is 0.5 which also indicates a rather high amount of contamination compared to the standard limit of 0.01 used for laser experiments in high vacuum environments [6] [15].

AFM analysis indicates the growth of the contamination layer on top of the coating. The edge of the irradiation site is thicker compared to the center, which agrees with the results of other research i.e. [7]. Besides the LIC phenomenon, the intense irradiation of the optical surface can also remove contamination. The pulse in the focal region reaches its peak intensity in the center. However, at the edges of the irradiating spot, the energy is insufficient for laser cleaning, so the contamination can accumulate more.

Simulations of ellipsometric parameters for “1L” experimental sample were performed using OTF Studio software [16] using different amorphous carbon thickness [17]. The optical parameters of carbon are shown in Fig. 12a). The growth of 3 nm of carbon increases the Delta and Psi values by 9 deg and 4 deg, respectively (see Fig. 12b). Such values are very similar to the measured results, which are demonstrated in Fig. 7. Absolute values are slightly different, which can be caused by deposition errors in the coating. Simulations results agrees with AFM measurements close to the edge of the LIC spot. Therefore it is reasonable to assume that contamination consists of 3 nm carbon layer around the irradiated area.

https://doi.org/10.1017/hpl.2025.10069 Published online by Cambridge University Press

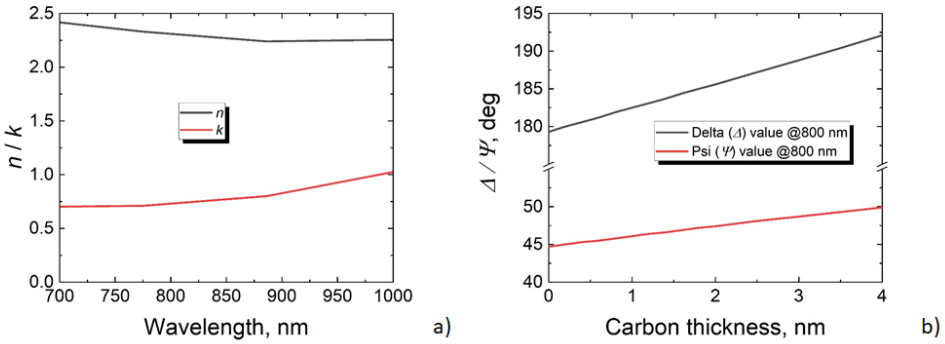

Fig. 12. Impact of ellipsometric Psi and Delta parameters values by the growth of a) amorphous carbon layer of b) different thickness.

Additional simulations were performed to evaluate the spectral reflectivity changes with and without the 3 nm amorphous carbon layer. Plots are presented in supplementary material, Fig. S5. Analysis indicates that changes in reflectance are large when E-field values at the surface are above zero. Reflectivity can drop to ~40 % due to large E-field enhancement for “1L” sample at the surface with absorbing carbon layer. Transmission remains the same and all losses in reflection are regarded as absorption. Changes in reflectance and transmittance for “0L” and “2L” experimental samples are minimal due to zero E-field enhancement at the surface. Reflectance measurements during the LIC are also presented in supplementary material, Fig. S4. Due to minimal detected changes or even registered increase in reflectivity for “1L” sample the data is considered unreliable. Despite that, we present our findings in supplementary and aim to modify the reflectivity measurement setup for the next research stage.

All the experimental samples were irradiated by a nearly identical diameter beam spot. Nevertheless, LIC affected areas had different sizes for each tested mirror. Each irradiation site was processed by ImageJ software and elliptical axes were evaluated. The results are plotted in Fig 13. As shown in the graph, the affected area of the LIC grows depending on the strength of electrical field enhancement. The major axis increased from 821 μm to 1223 μm, while the E-field level at the coating-vacuum interface raised from zero to 400 %. A similar tendency is observed for the minor axes, too. Two of the samples had the same E-field distribution at the surface. The lengths of the minor and major axes for the 0L and 2L samples are nearly identical. The LIC strongly depends on the peak intensity of laser pulses [9]. Ionization of hydrocarbons occurs at a certain intensity threshold. Therefore, when the light intensity is enhanced on the surface of a coating, larger area of the Gaussian beam can initiate the buildup of LIC.

The transverse profile of LIC features on the sample surface does not reproduce the focal spot profile. This could be caused, i.e., by space-charge effects during the transport of contamination from the rest gas to the sample surface or by subsequent action of the high intensity pulses (i.e. ablation, oxidation by residual singlet oxygen).

https://doi.org/10.1017/hpl.2025.10069 Published online by Cambridge University Press

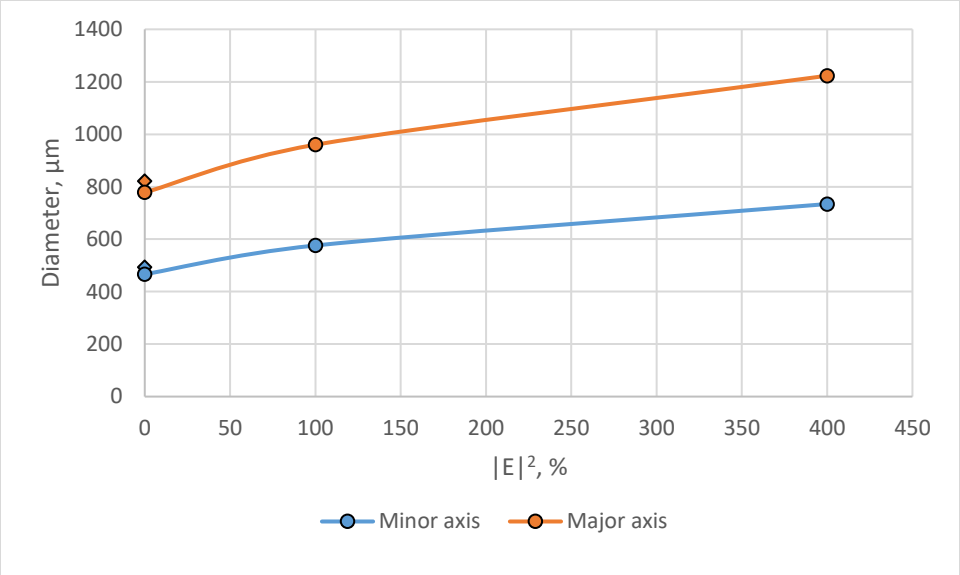

Fig. 13. Growth of LIC affected area for coatings with different E-field enhancement value on the top of coatings surface.

LIC can also lead to laser damage of the coatings i.e. due to absorption by the amorphous carbon. It is worth noting that laser induced discoloration can also be wrongly considered as contamination. Since laser induced damage threshold directly correlates to E-field enhancement in optical coatings, the optical coating with the largest E-field value at the interface between hafnia and silica will have the lowest laser induced damage threshold value. In our case such coating is the "1L" sample. Therefore, the experimental sample "1L" was ashed in an oxygen rich plasma for 24 hours (~60 W) after the experiment and measurements. After the ashing, no contamination was found on the sample, which confirms it was not the irreversible laser induced discoloration/damage. Additionally, it should be mentioned that LIC for the "0L" sample was barely detectable. Therefore, irradiation at 350 mJ/cm^2 is close to the threshold of LIC phenomenon for that sample.

The growth of LIC was observed for all the experimental samples. At the same time, strong evidence was presented for the mitigation of LIC by changing the design structure of high reflectivity mirrors, namely the top layer in our case. The area where the contamination layer is growing depends on spatial laser beam distribution and can be reduced by minimizing the E-field strength at the surface. The affected area further can be controlled by changing the material of the top layer. Contamination on silica surfaces has shown a tendency to have a higher impact compared to hafnia material. It can be related to dangling bonds of silanols, which are common for silica material [18]. Here presented investigation indicates that minimized E-field distribution and hafnia material as the last layer in the mirror has minimized the growth rate of LIC. Such approach can be used for other designs as well – polarizers, beam splitters, chirped mirrors etc. Currently we compared two top layer materials – hafnia and silica. In the future we plan to investigate more materials, coating designs and different deposition technologies.

https://doi.org/10.1017/hpl.2025.10069 Published online by Cambridge University Press

5. Conclusions

Long exposure under a high vacuum environment by fs laser radiation of electron beam deposited hafnia/silica mirrors clearly initiated LIC. Investigation of different multilayer designs revealed that contamination area size strongly depends on the surface E-field enhancement of the coating. Imaging ellipsometry measurements of irradiated sites showed that the smallest optical changes were initiated for the sample, which had a hafnia layer on top. The present research has demonstrated that laser induced contamination can be controlled by changing the multilayer coating design. Effective optimization of surface E-field values and appropriate material at the top of the coating stack can minimize the contamination growth for optical coatings in high power high intensity laser systems. Spectroscopic Imaging Ellipsometry provided a highly sensitive method for detecting and quantifying LIC, with variations in Δ (phase shift) and Ψ (reflectance ratio) serving as key optical markers. LIC effects extended beyond the primary Bragg reflection region, influencing the spectral response of the mirrors. This work provides critical insights for designing contamination-resistant coatings in high-power laser applications, particularly in industrial and space-based laser systems where optical longevity is crucial.

Funding. Research was funded from European Union of

IMPULSE project EU Horizon 2020 grant agreement No 871161

THRILL project EU HORIZON-INFRA-2022-TECH-01 grant agreement No 101095207.

SVM, SE, and JA acknowledge the project ADONIS (No. CZ.02.1.01/0.0/0.0/16-019/0000789) from the European Regional Development Fund.

Disclosures. The authors declare no conflicts of interest

References

[1] C. N. Danson, "Petawatt and exawatt class lasers worldwide," *High Power Laser Science and Engineering,* vol. 7, p. e54, 2019.

[2] D. Ristau, Laser-Induced Damage in Optical Materials, Boca Raton: CRC Press, 2014.

[3] S. Guizard, P. Martin, G. Petite, P. D'Oliviera and P. Meynadier, "Time-resolved study of laser-induced colour centres in SiO2," *Journal of Physics: Condensed Matter,* vol. 8, p. 1281, 1996.

[4] L. Smalakys, E. Drobužaitė, B. Momgaudis, R. Grigutis and A. Melninkaitis, "Quantitative investigation of laser-induced damage fatigue in HfO2 and ZrO2 single layer coatings," *Optics Express,* vol. 28, no. 17, pp. 25335-25345, 2020.

[5] T. J. Hollenshead, E. L. Klebanoff and G. Delgado, "Predicting radiation-induced carbon contamination of EUV optics," *Journal of Vacuum Science & Technology B,* p. 021602, 2019.

https://doi.org/10.1017/hpl.2025.10069 Published online by Cambridge University Press

[6] Z. Hubka, J. Novák, I. Majerová, J. T. Green, P. K. Velpula, R. Boge, R. Antipenkov, V. Šobr, D. Kramer, K. Majer, J. A. Naylon, P. Bakule and B. Rus, "Mitigation of laser-induced contamination in vacuum in high-repetition-rate high-peak-power laser systems," *Applied Optics,* vol. 60, no. 3, pp. 533-538, 2021.

[7] M. Hippler, P. Wagner, H. Schroeder and W. Riede, "Laser-induced contamination of space borne laser systems: impact of organic contamination and mitigation by oxygen," *Proc. SPIE 9952, Systems Contamination: Prediction, Control, and Performance 2016,* p. 99520N, 2016.

[8] M. Stehlík, "Laser damage resistance of coating materials and structures for grating-waveguides," PhD Thesis, 2022.

[9] F. R. Wagner, "Laser induced deposits in contaminated vacuum environment: Optical properties and lateral growth," *Optics & Laser Technology,* vol. 122, p. 105889, 2020.

[10] G. Abromavicius, R. Buzelis, R. Drazdys, A. Melninkaitis and V. Sirutkaitis, "Influence of electric field distribution on laser induced damage threshold and morphology of high reflectance optical coatings," *Laser-Induced Damage in Optical Materials: 2007,* vol. 6720, p. 67200Y, 2007.

[11] M. Jupé, M. Lappschies, L. Jensen, K. Starke, D. Ristau, A. Melninkaitis, V. Sirutkaitis, I. Cravetchi and W. Rudolph, "Mixed oxide coatings for advanced fs-laser applications," *Laser-Induced Damage in Optical Materials: 2007,* vol. 6720, p. 67200U, 2007.

[12] P. Drude, "Ueber Oberflächenschichten. I. Theil," *annalen der physik,* vol. 272, no. 2, p. 532–560, 1889.

[13] R. M. A. Bashara and N. M. Azzam, Ellipsometry and polarized light, New York: North-Holland: Elsevier Science Pub. Co., 1987.

[14] G. H. Tompkins and A. E. Irene, Handbook of ellipsometry, Heidelberg, Germany: William Andrew Pub., 2005.

[15] LIGO, "LIGO document E080177-v2: RGA test qualification of components for the LIGO UHV," 2020.

[16] M. Trubetskov, "OTF Studio Thin Film Software," 2025. [Online]. Available: https://www.otfstudio.com.

[17] E. T. Arakawa, M. W. Williams and I. T., "Optical properties of arc-evaporated carbon films between 0.6 and 3.8 eV," *J. Appl. Phys.,* pp. 3176-3177, 1977.

[18] L. T. Zhuravlev and V. V. Potapov, "Density of silanol groups on the surface of silica precipitated from a hydrothermal solution," *Physical Chemistry of Surface Phenomena,* vol. 80, pp. 1119-1128, 2006.

https://doi.org/10.1017/hpl.2025.10069 Published online by Cambridge University Press